J Mol Model (2014) 20:2448
DOI 10.1007/s00894-014-2448-5

ORIGINAL PAPER

Comparative density functional theory based study of the reactivity of Cu, Ag, and Au nanoparticles and of (111) surfaces toward CO oxidation and NO_2 reduction

B. Pascucci · G. S. Otero · P. G. Belelli · F. Illas · M. M. Branda

Received: 27 February 2014 / Accepted: 26 August 2014

Abstract The reactivity of Cu, Ag, and Au nanoparticles and of the corresponding (111) surfaces of these elements toward CO oxidation and NO_2 reduction has been investigated by means of DFT and DFT-D calculations. The co-adsorption energies of CO and O on Ag and Au surfaces are smaller than that corresponding to Cu surface but the oxidation reaction is energetically more favored for the heavier metals. The adsorption energy of NO_2, E_{ads}, is about 50 % larger on nanoparticles than on the metal perfect surfaces, following the almost general rule stating that the lower coordinated sites are those where the interaction is the largest. Interestingly for the co-adsorption and oxidation of CO an increase of reactivity is found for the Au nanoparticles, which is attributed to the large number of low coordinated sites due to the specific shape of this nanoparticle induced by the adsorbates.

Keywords Adsorption · Catalysts · DFT-D · Metal nanoparticles

Introduction

Two of the most dangerous and noxious atmospheric pollutants are NO_x and CO which are produced in the combustion of fossil fuels either through incomplete combustion or because of the presence of traces of elemental nitrogen. The former is responsible for acid rain whereas CO is harmful to human health because it binds to Fe hemoglobin thus hindering arrival of oxygen to vital organs. For these reasons, NO_x catalytic reduction and CO oxidation reactions have long been studied and more recently attracted the attention of several groups investigating the catalytic properties of Au nanoparticles. Catalysis by Au nanoparticles is a field of enormous interest triggered by the independent works of Haruta [1] and Goodman [2] and followed by many other groups [3–6]. Today it is very well known that Au in the form of small clusters or finely dispersed on metal oxides exhibits high catalytic activity toward oxidation processes at mild temperature. It has also been found that, compared to the commonly used oxide supports, Au nanoparticles supported on TiC have even better catalytic properties for CO oxidation, desulfurization, and hydrogenation reactions [7]. Besides, Au, Cu, and Ni nanoparticles supported on TiC are very active for CO_2 hydrogenation to methanol and methane [8].

An important question regarding these experiments concerns the reactivity of metallic nanoparticles compared to that of extended surfaces. This comes from the fact that the experimental studies of Goodman et al. [2, 9] using a variety of surface science techniques, including scanning tunneling microscopy/spectroscopy (STM/STS) and elevated pressure reaction kinetics measurements on Au clusters ranging in diameter from 1 to 6 nm, show that the structure sensitivity of this reaction is related to a quantum size effect with respect to the thickness of the gold islands; islands with two Au layers are most effective for catalyzing the oxidation of CO. Even smaller particles are those found to be active when supported on TiC [7]. Likewise, from theoretical calculations, Hvolbæk et al. [10] have found that Au nanoparticles with less than 3–5 nm in diameter are catalytically active for several chemical reactions. These authors find that the fraction of low-coordinated Au atoms scales approximately with the catalytic

This paper belongs to Topical Collection QUITEL 2013

B. Pascucci · G. S. Otero · P. G. Belelli · M. M. Branda (✉)
Instituto de Física del Sur, CONICET y Departamento de Física, Universidad Nacional del Sur, Av. Alem 1253, 8000 Bahía Blanca, Argentina
e-mail: cabranda@criba.edu.ar

F. Illas
Departament de Química Física & Institut de Química Teòrica i Computacional (IQTCUB), Universitat de Barcelona, C/ Martí i Franquès 1, 08028 Barcelona, Spain

Published online: 11 September 2014

activity, suggesting that atoms on the corners and edges of Au nanoparticles are the active sites. However, theoretical studies carried out by Roldán et al. [11, 12] for the dissociation of O_2 on Au nanoparticles showed convincing evidence that, in addition to the presence of low coordinated Au atoms, there is a critical size for Au nanoparticles for this reaction to happen. They concluded that the catalytic effect observed by Lambert et al. [13] about the epoxidation of styrene by dioxygen on Au nanoparticles derived from Au_{55} supported on SiO_2 is likely to be catalyzed by a minority of smaller particles. Clearly, a systematic study comparing the activity of nanoparticles and extended surfaces is needed.

In the case of extended surfaces there is abundant literature regarding the adsorption of CO and NO. Hence, the interaction of NO with the (111) surface of transition metals has been studied by Gajdoš et al. [14] who found that the adsorption on Cu and Ag occurs preferentially on hcp-hollow sites whereas on Au(111) the authors found a very weak adsorption only on bridge-sites. These authors also studied NO dissociation and report a relationship between adsorption and activation energy [15]. Torres et al. [16] studied the adsorption of NO on two models of Au(111) substrate, one slab with four layers and the other with two layers, to account for effects of the reduced thickness of the substrate. They found an adsorption energy of NO on a clean regular Au(111) surface of about 0.21 eV. They also suggested that NO_2 formation from NO on regular sites of Au(111) surface will be limited by the lifetime of the weakly bound NO species. Moreover, these authors found that O atoms preadsorbed on the surface enhance adsorption of NO and the (NO + O)/Au(111) complexes and transform into NO_2/Au(111) products without an activation barrier. The electronic properties with respect to the adsorption and oxidation of NO found on a regular Au(111) surface and a supported thin film are qualitatively the same, which was also shown experimentally in the case of CO adsorption [17]. The magnitude of the interaction between NO and/or O and the underlying surface is very important since it determines its potential chemical activity. This is clear from the kinetic Monte Carlo simulations of NO oxidation on Pt(111) using DFT parameters [18]. These calculations have shown that the NO + O/NO_2 reaction is inhibited rather than promoted on Pt(111), due to strong oxygen–platinum bonds. Only at sufficiently high oxygen chemical potential does Pt become an efficient oxidation catalyst, as Pt-O bonds are weakened with increasing coverage, and the NO_2 formation reaction becomes exothermic. At that point, Pt catalyzes the reaction by lowering the activation barrier for the kinetic reaction. These results are congruent with flow-reactor experiments [18].

From a fundamental point of view, the reactivity of metallic nanoparticles has been much less studied even if they are a key component in supported heterogeneous catalysts [19–21]. These systems exhibit physical and chemical properties which are significantly different from those of the bulk and of the perfect extended surfaces [22]. One of the main conclusions extracted from the specific literature is that the particle size plays an important role in improving their catalytic activity. In order to better understand the effect of the lower coordination sites present on nanoparticles, NO_2 decomposition to NO + O and CO + O oxidation to CO_2 catalyzed by small octahedral nanoparticles of Cu, Ag, and Au has been theoretically studied and the energy profile compared to that corresponding one for extended (111) surfaces. From this comparison we will show that, as expected, all species interact more strongly with the nanoparticles, a behavior which is attributed to the larger reactivity of the low coordinated sites. Moreover, the activity of the Au nanoparticle is significantly different, the reason being the facility to change its shape in response to the presence of adsorbed species.

Computational details

In this work, the geometrical structure and reactivity of Cu_{19}, Ag_{19}, and Au_{19} octahedral nanoparticles toward NO_2 decomposition and CO oxidation is studied and compared to that of the corresponding (111) perfect surfaces. Based on the empirical Brønsted–Evans–Polanyi relationship [23, 24], which establishes a linear relationship between the activation energy and the reaction energy, we consider the reaction energy values as a good descriptor of the substrate activity. In this way, we follow previous works which have established the validity of these BEP relationships in a variety of heterogeneously catalyzed reactions taking place on a range of different substrates [25–27]. These BEP relationships are also useful in providing accurate, simple descriptors of the catalytic activity [28–30]. To further check the validity of the BEP relationships in the cases studied in the present work, we have explicitly considered the energy barriers for NO_2 reduction reaction on the three perfect surfaces by appropriate transition state structure location and characterization by frequency analysis. The results from these calculations fully validate the hypothesis behind the BEP relationships.

The overall study is supported on periodic density functional theory (DFT) based calculations carried out using the *Vienna* Ab-Initioo *Simulation Package* (VASP) [31–35]. This code solves the Kohn-Sham equations for the valence electron density within a plane wave basis set and makes use of the projector augmented wave (PAW) method to describe the interaction between the valence electrons and the atomic cores, including scalar relativistic effects for the metal atoms [36]. A cutoff of 415 eV for the kinetic energy of the plane waves in the basis set has been used which allowed a convergence up to 10^{-3} eV in the total force. The calculations of N or O atoms were always performed at the spin-polarized level.

The calculations have been carried out using the PW91, [37, 38] and/or PBE [39] forms of the exchange correlation

potential. Note that both forms of the generalized gradient approximation (GGA) provide a good compromise for accuracy versus computational cost and have shown to lead a robust description of all transition metal elements series [40]. In spite of the good performance of these functionals in describing bulk metals, one can still claim that hybrid functionals are needed to describe the thermochemistry of reactions involving main elements as is the case for CO, NO, or O adsorption here (see [41] and references therein). These arguments are no doubt correct but one must realize that using hybrid functionals to describe the metallic systems also faces important problems [42]. In fact, in a very recent work it has been shown that hybrid functionals do not overcome the performance of GGA in describing the properties of bulk metals which constitutes a clear challenge in the search of universal functionals [43]. Hence, the choice of the GGA functionals in this work represents a compromise between accuracy in the description of the main elements chemistry and of metallic systems and most often constitutes the common choice in the literature regarding these systems.

In order to investigate the influence of dispersion, the structures and energies for the CO oxidation were also evaluated at the DFT-D level with the approximation suggested by Grimme [44] added to the PBE calculated energy. In the DFT-D approach, the total energy is given by:

$$E^{(DFT-D)} = E^{DFT} + E_{disp} \quad (1)$$

where E^{DFT} is the Kohn–Sham total energy as obtained from genuine PBE and E_{disp} is an empirical dispersion correction given by:

$$E_{disp} = -s_6 \sum_{i,j} f(R_{ij}) C_6^{ij} (R_{ij})^{-6} \quad (2)$$

where f (R_{ij})represents a damping function and the C_6^{ij} coefficients are obtained from atomic polarizabilities and ionization potentials. On the other hand, s_6 is a scaling factor which was optimized in 0.75 for PBE [44].

Octahedral nanoparticles containing 19 atoms (M_{19}) were employed as suitable realistic models because these exhibit atoms with low coordination number, exhibit well defined (111) facets, contain core atoms with bulk coordination and have an overall size that maintains calculations feasible with a reasonable computational cost. It is also important to point out that the structure of the particle is cut from the bulk as in previous works dealing with coinage nanoparticles [45] and, accordingly, it may not represent the global minimum for this number of atoms. Precisely, cutting the structure from the bulk and relaxing it guarantees that the particle mimics larger octahedral particles and not the most stable structure of a gas phase cluster [22].

Possible adsorption sites for all the studied species on the nanoparticles are shown in Fig. 1. The M(111) surfaces were represented by slabs with a periodic structure along the surface including five layers. The sizes of the surface unit cells were chosen of 2×2 and 3×3 to represent coverage values of 0.25 and 0.11, respectively. Numerical integration in the reciprocal space was carried out using 5×5×1 Monkhorst-Pack special *k*-points grids [46] for the two supercells representing the perfect (111) surface, whereas calculations for the nanoparticles have been carried out at the Γ point only.

Results and discussion

$CO+½\ O_2 \rightarrow CO_2$reaction

In order to compare the different performance of DFT and DFT + D we first consider CO adsorption on the (111) metal surfaces with a coverage Θ=0.25. Table 1 reports the calculated adsorption energy values (E_{ads}) obtained by PBE-vdW and PW91 (between brackets). Note that both PBE and PW91 functionals provide almost the same results for the properties of the three transition metal series providing the best agreement with experimental data [40]. It is also worth pointing out that the energy profile for water dissociation predicted by these two GGA type functionals is almost the same. Therefore, one could safely argue that comparing PW91 with PBE-vdW is almost the same as comparing PBE with PBE-vdW [47].

From Table 1 we can observe that, not unexpectedly, the calculations without dispersion corrections give values close to zero incorrectly predicting that CO would not adsorb on these surfaces. However, the results absolutely change when the dispersion correction is included. Since experimental

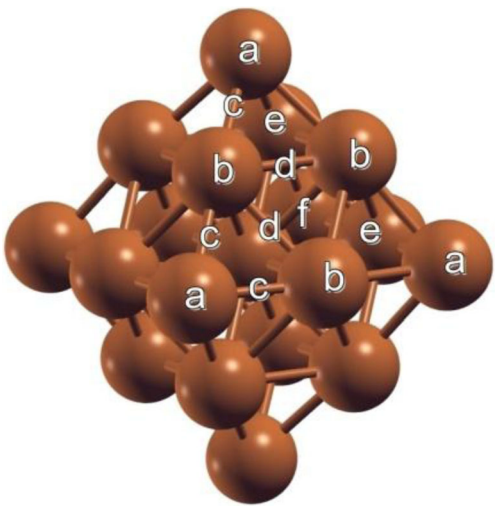

Fig. 1 Possible adsorption sites for all studied species on the metal M_{19} nanoparticles

Table 1 CO adsorption energy (in eV) on (111) perfect surfaces calculated by PBE-vdW and (PW91) approaches and as in Eq. 3. The most favorable cases are marked in bold

Θ=0.25	COt	COb	COh	Exp. data
Cu	−0.94 (+0.06)	−0.99 (−0.01)	**−1.07** (−0.01)	−0.49 [48]
				−0.52 [49]
Ag	−0.38 (0.00)	−0.37 (0.00)	**−0.39** (0.00)	−0.28 [50]
Au	−0.52 (0.00)	**−0.53** (0.00)	−0.49 (0.00)	−0.40 [51]

results for CO adsorption on Cu(111) [48, 49], on Ag(111) [50], and on Au(111) [51] consistently report adsorption energy values in the 0.3–0.5 eV range (see Table 1), we conclude that these calculations must be carried out including the van der Waals corrections even if the empirical approach by Grimme [44] slightly overestimates the adsorption energy values. Nevertheless, this approach agrees with the experimental results on the order of adsorption strength toward CO; Cu>Au>Ag. Therefore all following calculations about the CO oxidation were carried out using dispersion corrections.

Consistent with the findings above, the study of the CO oxidation reaction on nanoparticles of Cu, Ag, Au and on the respective extended (111) surfaces was carried out at the DFT + D level using the PBE [39] form of the exchange correlation potential with the approximation suggested by Grimme [44]. In all cases, the co-adsorption of CO and O species was explored by considering all possible combinations of surface adsorption sites. Tables 2 and 3 show the results found for the perfect (111) surfaces and for the M_{19} (M = Cu, Ag, Au) nanoparticles, respectively. These values were calculated with respect to gaseous CO and O_2 molecules, that is:

$$E_{co-ads}(CO + O) = E(CO + O/MS) - E(MS) - E(CO) - {}^{1/2}E(O_2) \quad (3)$$

where E(CO + O/MS) is the total energy of CO and O co-adsorbed on the metallic substrate (MS), E(MS) is the energy of the clean MS and E(CO), and $E(O_2)$ the total energy of the gas phase molecules in their electronic ground state (closed shell singlet for CO and triplet state for O_2). This is a common choice for the reference energy which avoids large

Table 2 CO + O co-adsorption energy (in eV) on (111) perfect surfaces calculated by PBE-vdW as in Eq. 3. The most favorable cases are marked in bold

	COt + Oh	COb + Oh	COh + Ob
Cu	**−3.41**	–	–
Ag	**−1.76**	−1.31	–
Au	**−1.50**	−0.88	−1.18

Table 3 CO + O co-adsorption energy (in eV) on metal nanoparticles calculated by PBE-vdW as in Eq. 3. The most favorable cases are marked in bold

	COa		COd			COe	
	Od	Oe	Oa	Oc	Oe	Oa	Oc
Cu	–	**−3.40**	–	–	−3.19	−1.84	–
Ag	−1.49	**−1.72**	–	–	–	–	−0.96
Au	−2.04	**−2.26**	−1.29	−1.53	−2.03	–	–

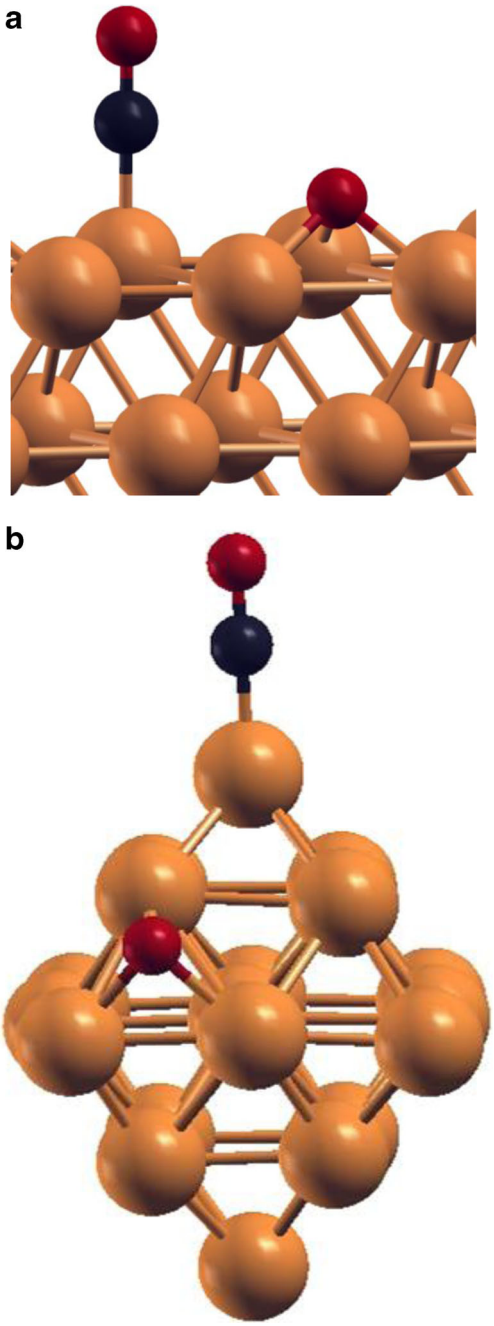

Fig. 2 **a** COt + Oh co-adsorbed on Cu(111) and **b** COa + Oe co-adsorbed on Cu nanoparticle. C: *black sphere*, O atoms: *red spheres*, and Cu: *brown sphere*

Table 4 CO_2 adsorption energy (in eV) on (111) perfect surfaces calculated by PBE-vdW and (PW91) approaches (see Eq. 4). The most favorable cases are marked in bold

Θ=0.25	CO_2 t	CO_2 b	CO_2 h
Cu	−0.19(−0.06)	−0.17 (+0.03)	**−0.24** (+0.05)
Ag	**−0,23**(−0.08)	−0.17 (−0.09)	**−0.23** (−0.07)
Au	−0.23(+0.01)	**−0.31** (+0.04)	−0.27 (0.00)

error in the dissociation of the oxygen molecule in the gas phase as predicted by the PW91 or PBE functionals. However, taking into account that Eq. 3 does not consider the dissociation energy of O_2, the calculated values can be used to compare the different systems but do not provide absolute adsorption energy values. In this way, one can readily see that COt + Oh is the preferred combination of surface sites for the three metal surfaces and also for the nanoparticles (see Figs. 2a and b). The existence of low coordinated sites such as corners and edges on the nanoparticles provides additional adsorption sites. The summary of results for co-adsorption is reported in Tables 2 and 3. Even though the reactivity of CO on metal surfaces follows the Cu>Au>Ag order, as was shown in Table 1, this trend changes to Cu>Ag>Au when an oxygen is co-adsorbed on these surfaces (see Table 2). This change is not unexpected taking into account that the oxidation potential of Au is larger than that of Cu and Ag and, therefore, Cu and Ag are easier to oxidize than Au. However, the co-adsorption energies on nanoparticles follow the Cu>Au>Ag order and here the major increase of reactivity of Au compared to Ag is due to the appearance of additional low coordination sites which is triggered by the presence of the adsorbates. This behavior indicates an interesting restructuration of Au_{19} nanoparticle, which is in agreement with previous results obtained by Beret et al. [52] when CO is adsorbed on Au_{13} nanoparticle.

Regarding CO_2 adsorption on different sites of (111) surfaces and on nanoparticles, Tables 4 and 5 report adsorption energy values calculated from DFT and DFT + D. These values were calculated as follows:

$$E_{ads}(CO_2) = E(CO_2/MS) - E(MS) - E(CO_2) \quad (4)$$

where $E(CO_2/MS)$ is the total energy of CO_2 adsorbed on the metallic substrate MS, E(MS) is the energy of the clean MS and $E(CO_2)$ the total energy of the gas phase molecule. A CO_2 adsorption mode with the O atom pointing to the metal surfaces is possible and has been explored although the final

Table 5 CO_2 adsorption energy (in eV) on metal nanoparticles calculated by PBE-vdW approach (see Eq. 4)

	CO_2 a	CO_2 d	CO_2 e
Cu	−0.08	−0.13	−0.16
Ag	−0.12	−0.18	−0.18
Au	−0.10	−0.20	−0.20

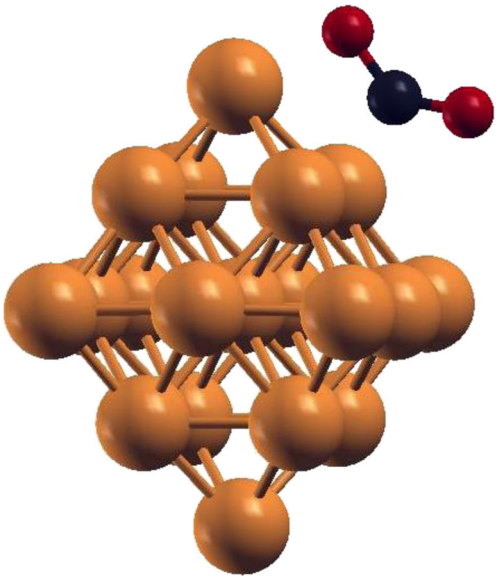

Fig. 3 CO_2d on Cu_{19} with an OCO angle equal to 137°. C: *black sphere*, O atoms: *red spheres*, and Cu: *brown sphere*

situations is highly unstable and, hence, not further commented.

Once again DFT without dispersion does not show any noticeable interaction between the surface and the molecule. Calculations carried out with PBE + vdW approach show E_{ads} between 0.2 and 0.3 eV on (111) surfaces and between 0.1 and 0.2 eV on nanoparticles. Therefore, from these results the CO_2 desorption is easy on surfaces and even more on nanoparticles. A larger value has been reported for the CO_2 adsorption energy although using a very small Au_2. This is not surprising since the coordination number of Au atoms in Au_2 and in the octahedral Au_{19} nanoparticle model is very different [53]. For all (111) surface sites and for most of the sites of the nanoparticles, the O-C-O angle of the adsorbed molecules predicted by geometrical optimization was practically equal to 180° which indicates that the CO_2 molecule is not activated. However, on the d and e sites of the Cu nanoparticle this angle noticeably changes to ~140° (see Fig. 3) and the molecule gets significantly close to the metallic substrate. This chemical interaction is not evident looking at the adsorption energy values only, but this apparent incongruence can be understood having in mind that to deform the CO_2 molecule also implies an energy cost. A similar behavior has been observed for CO_2 adsorbed on Cu/TiC and Au/TiC, [8] on Pd(111) [54] and it also plays a role in the adsorption of methanol on MgO [55].

Table 6 Oxidation reaction energy (in eV) of CO on (111) perfect surfaces (see Eq. 5). The most favorable cases are marked in bold

Θ=0.25	COtOh CO_2t	CObOh CO_2b	COhOb CO_2h
Cu	−0.57	–	–
Ag	−2.26	**−2.66**	–
Au	−2.53	–	**−2.86**

Table 7 Oxidation reaction energy (in eV) of CO on metal nanoparticles (see Eq. 5). The most favorable cases are marked in bold

	CO_2a		CO_2d			CO_2e	
	COa		COd			COe	
	Od	Oe	Oa	Oc	Oe	Oa	Oc
Cu	–	−0.37	–	–	−0.53	**−1.57**	–
Ag	−2.36	−2.11	–	–	–	–	**−2.99**
Au	−2.05	−1.61	**−2.70**	−2.34	−1.50	–	–

For the oxidation reaction, the thermodynamic balance has been calculated as in Eq. 5 below and reported in Tables 6 and 7 for the (111) surfaces and nanoparticles, respectively.

$$E_{reac} = E(CO_2/MS) - E(CO + O/MS) \quad (5)$$

From Tables 6 and 7 it clearly appears that the order of E_{reac} for the (111) surface follows the Au>Ag>Cu trend on (111) surfaces whereas it changes to Ag>Au>Cu for the M_{19} nanoparticles. The E_{reac} negative values indicate that the CO_2 formation is energetically favorable, from CO+O, both on the metal surfaces and nanoparticles.

As commented before for the Cu surface, the co-adsorption energies are significantly large on COtOh configuration, ~ −3.4 eV (see Tables 2 and 3), but the respective oxidation energies corresponding to this initial configuration of the reactants —~ −0.4 eV/−0.6 eV (see Tables 6 and 7)— are not the most favorable. On the other hand, even though the co-adsorption energies on Ag and Au surfaces are smaller than that corresponding to Cu(111), the oxidation reaction is, however, much more energetically favored.

For the Cu nanoparticle, the largest E_{reac}(CO) corresponds to the COe+Oa configuration of the reactants although this is not the more likely combination of adsorption sites of the individual species. A similar situation is found in the case of the Ag nanoparticle where the largest oxidation energy occurs from COe+Oc but, again, this does not correspond to the most stable combination of adsorption sites of isolated species. However, the oxidation energies arising from the COa+Od and COa+Oe initial states (Fig. 4a and b) are also quite large and these effectively correspond to the most probable adsorption sites. For the Au nanoparticle, the preferential sites are COa+Od, COa+Oe, and COd+Oe (Fig. 5a, b, and c), as was displayed in Table 3, and these are also very reactive sites toward the oxidation (see Table 7).

$NO_2 \rightarrow NO + ½\ O_2$ reaction

The dissociation of NO_2 on M(111) (*M*=Cu, Ag, and Au) perfect surfaces and on the respective M_{19} nanoparticles has been studied following the same approach as for the CO oxidation reaction. In a preliminary set of calculations, the NO_2 adsorption energies on the (111) surfaces were calculated as in Eq. 6 below by imposing a coverage Θ=0.25 and with the N atom pointing toward the surface, the corresponding results are reported in Table 8.

$$E_{ads}(NO_2) = E(NO_2/MS) - E(MS) - E(NO_2) \quad (6)$$

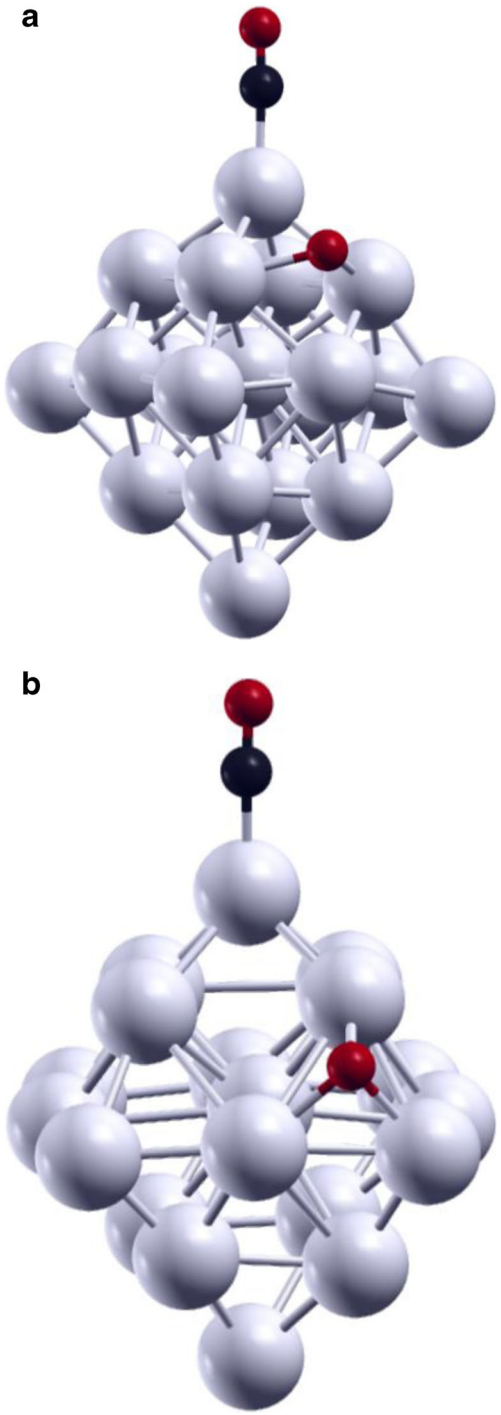

Fig. 4 **a** COa + Od/Ag_{19} and **b** COa + Oe/Ag_{19}. C: *black sphere*, O atoms: *red spheres*, and Ag: *white sphere*

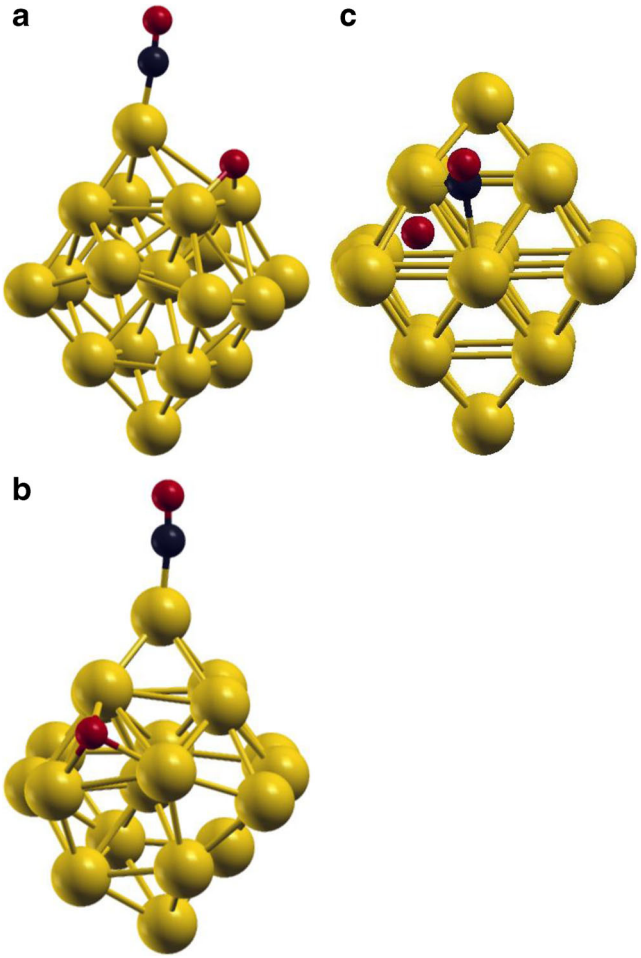

Fig. 5 **a** CO$_a$ + Od/Au$_{19}$, **b** CO$_a$ + Oe/Au$_{19}$ and **c** CO$_d$ + Oe/Au$_{19}$. C: *black sphere*, O atoms: *red spheres*, and Au: *yellow* sphere

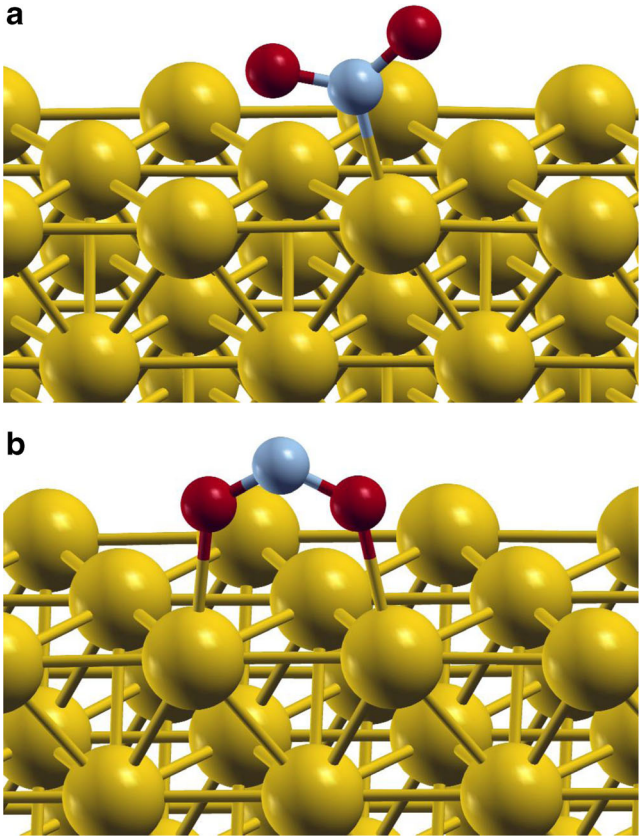

Fig. 6 **a** NO$_2$t/Au(111) and **b** NO$_2$(inv)/Au(111). N: *light blue sphere*, O atoms: *red spheres*, and Au: *yellow spheres*

From these calculations it follows that interaction of NO_2 directly at the top site is the most favored (see Fig. 6a). Moreover, for the three metallic surfaces, adsorption energy is larger at the top site (T) than on the hollow (H) which is larger than at the bridge (B) site. Considering that T is the preferred site for the NO_2 on these surfaces, the situation with smaller coverage was also considered, represented by a suitable larger supercell. Thus, the NO_2 adsorption at T was analyzed at the smaller coverage (Θ=0.11) but the upside-down orientation with the O atoms pointing toward the surface was also considered (Fig. 6b) which is referred to as NO_2(inv). From the energy values shown in Table 8, it appears that the upside-down orientation is indeed the most favorable. We can see that the adsorption order is Cu>Ag>Au. The adsorption energies of NO_2 on nanoparticles also calculated as in Eq. 6 are exposed in Table 9. The order of stability is the same as in the (111) surface. The most favorable position is also the upside-down sites, but now two possible stable sites (a and b) are possible for the N-down orientation (see Fig. 7a and b). These values are approximately 50 % larger than on the metal perfect surfaces, following the almost general rule: the lower coordinated sites are those where the interaction is the strongest.

Table 8 NO_2 adsorption energy (in eV) on (111) metal surfaces calculated by PW91 approach. The most favorable cases are marked in bold

	E_{ads} NO_2				
	NO_2 (T)		NO_2 (B)	NO_2 (H)*	NO_2 inv
	Θ=0.25	Θ=0.11	Θ=0.25	Θ=0.25	Θ=0.11
Cu	−1.11	**−1.32**	−0.42	−0.71	**−1.51**
Ag	−0.83	**−0.95**	−0.45	−0.62	**−1.18**
Au	−0.42	**−0.52**	0.11	−0.23	**−0.74**

*Hollow HCP and FCC gave the same energies

Table 9 NO_2 adsorption energy (in eV) on metal nanoparticles calculated by PW91 approach. The most favorable cases are marked in bold

	NO_2a	NO_2b	NO_2(inv)
Cu	−2.03	−2.07	**−2.31**
Ag	−1.47	−1.49	**−1.74**
Au	−1.31	−1.29	**−1.50**

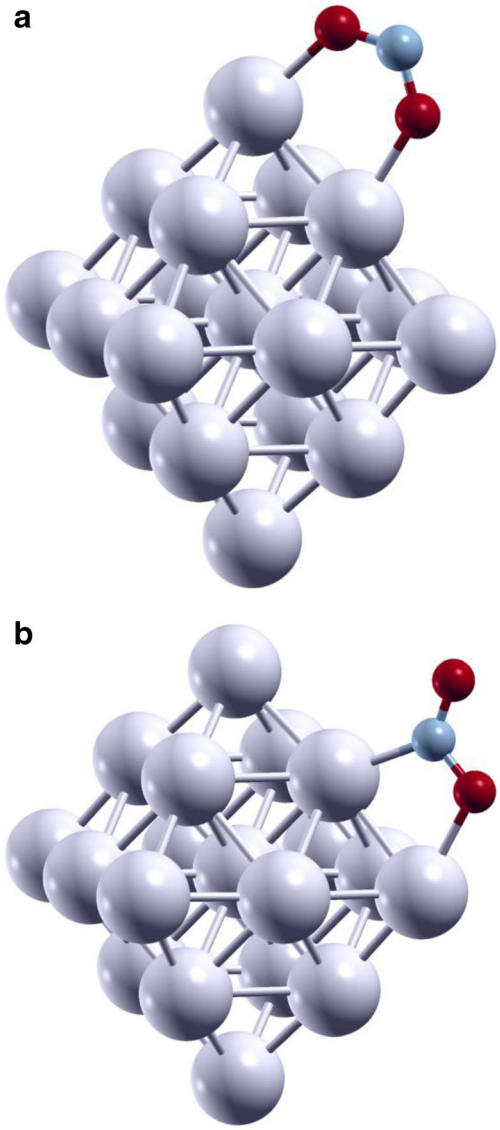

Fig. 7 **a** NO_2(inv)/Ag_{19} and **b**NO_2b/Ag_{19}. N: *light blue sphere*, O atoms: *red spheres*, and Ag: *white spheres*

From the more stable NO_2 adsorption sites the dissociation toward NO+O was studied for the Θ=0.11 coverage using a 3×3 supercell. The dissociation energy was calculated as in Eq. 7

$$E_{dis}(NO_2/MS) = E(NO + O/MS) - E(NO_2/MS) \quad (7)$$

Table 10 Dissociation reaction energy (in eV) of NO_2 on (111) perfect surfaces with Θ=0.11 calculated by PW91 approach

Θ=0.11	NO_2t		NO_2(inv)	
	NOtOfcc	NOtOhcp	NOtOfcc	NOhcpOfcc
Cu	0.19	0.33	0.31	−0.05
Ag	1.26	1.34	1.51	1.47
Au	1.25	1.50	1.48	–

Table 11 Dissociation reaction energy (in eV) of NO_2 on metal nanoparticles calculated by PW91 approach

	NO_2(inv)				
	NOa + Oe	NOc + Oc	NOc + Oe	NOb + Oe	NOe + Oe
Cu	0.50	0.49	0.24	–	0.23
Ag	1.75	–	1.89	2.20	–
Au	1.53	1.51	–	–	–

where the definitions are equivalent to those in Eq. 5. In order to properly compute the reaction energy corresponding to NO_2 dissociation, all possible combinations of NO and O co-adsorption sites were considered and analyzed. Several combinations, however, led to the NO_2 molecule. The E_{dis} values for the M(111) surfaces and M_{19} nanoparticles are reported in Tables 10 and 11, respectively. Except in the case of the situation NO_2(inv)→NOhcp + Ofcc in Fig. 8, all the reactions are endothermic. The difference between the E_{dis} value for the reaction on Cu(111) and on Ag(111) and Au(111) is significant. For Cu(111), E_{dis} values are between −0.05 and 0.33 eV, depending on the atomic configuration. However, values larger by 1 eV are found for Ag(111) and Au(111) as clearly seen in Table 10. Here we must underline that although NO_2(inv) on Cu surface is found to be quite stable (see Table 8), the

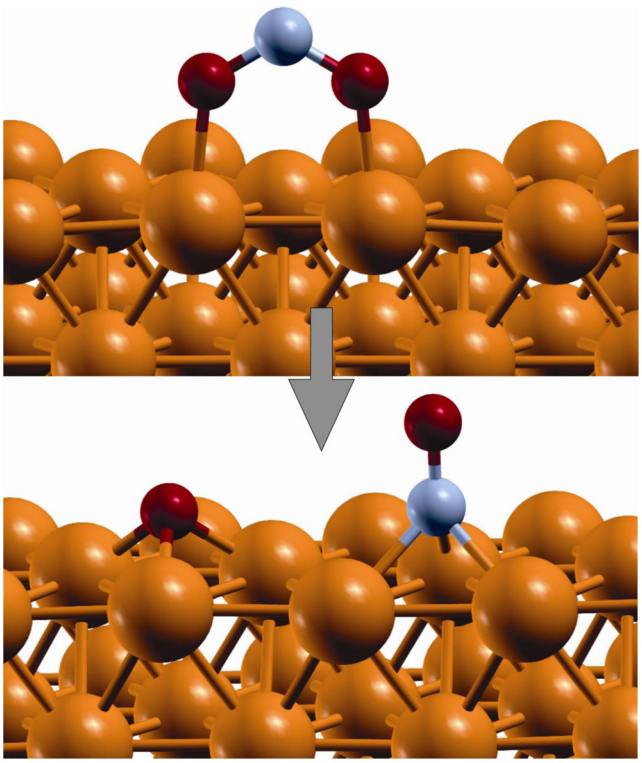

Fig. 8 NO_2(inv)/Cu(111)→NOhcp+Ofcc/Cu(111). N: *light blue sphere*, O atoms: *red spheres*, and Cu: *brown spheres*

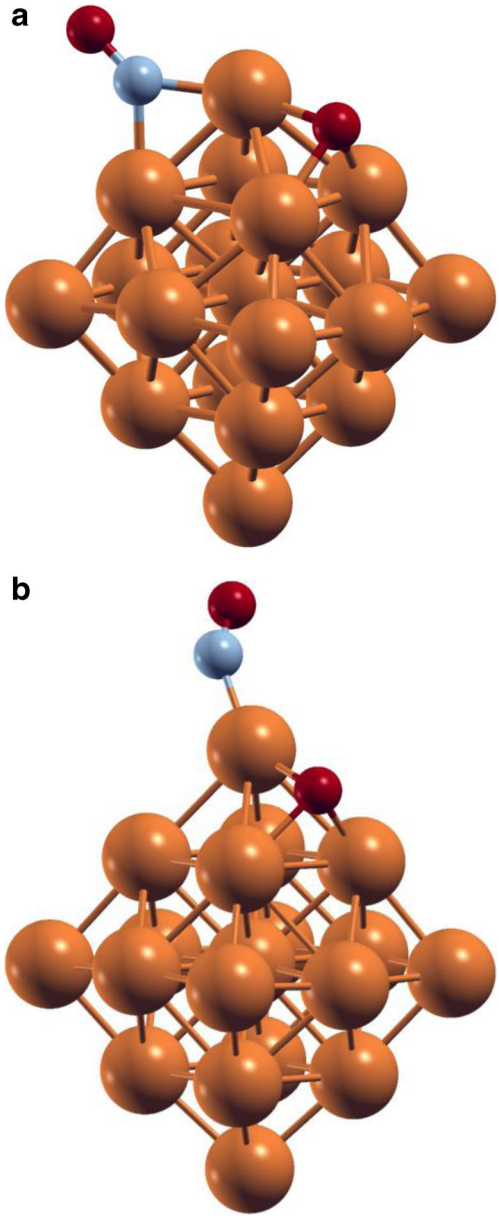

Fig. 9 NOc+Oe/Cu_{19} and NOa+Oe/Cu_{19}. N: *light blue sphere*, O atoms: *red spheres*, and Cu: *brown spheres*

calculated E_{dis} value indicates a favorable trend for the dissociation of the adsorbed molecule.

On the M_{19} nanoparticles a large number of co-adsorption sites was considered but only those more favorable for the dissociation reaction are displayed in Table 11. Again the most reactive metal resulted to be Cu, with E_{dis} ~0.2 and 0.5 eV in the cases of NOc + Oe and NOa + Oe (see Fig. 9a and b), respectively. On the other hand, all the reaction energies calculated for Ag and Au nanoparticles are between 1.5 and 2.2 eV. Once again, Au nanoparticles show reactivity higher than Ag (see Table 7 about CO oxidation) which is due to the higher facility of the former to deform in the presence of adsorbate.

Conclusions

Periodic density functional theory based calculations including dispersion terms reveal that CO adsorption and oxidation on M(111) surfaces and M_{19} nanoparticles (*M*=Cu, Ag, and Au) should include van der Waals corrections. The preferred pair of co-adsorption sites for CO and O is on top and on hollow, respectively, for the three metal surfaces and also for the nanoparticles. Interestingly, while the co-adsorption energies of CO+O on Ag and Au surfaces are smaller than that corresponding to Cu surface, the oxidation reaction is, however, much more energetically favored. Likewise, an increase of reactivity is found for the Au nanoparticle which is attributed to the larger quantities of low coordinated sites on this particle in the presence of the adsorbates.

In the case of NO_2 adsorption and dissociation on the same systems, the most likely adsorption configuration for the NO_2 molecule implies an upside-down orientation with the O atoms pointing toward the surface or an on top adsorption with the N atom bound to the surface. The calculated dissociation energy for adsorbed NO_2 on the nanoparticles is 50 % larger than on the metal perfect surfaces which is at variance from the trend found for CO_2 dissociation, the reverse of the CO+O reaction. The difference in calculated $E_{dis}(NO_2)$ values on Cu and on Ag and Au provides an indication of the expected trend for the dissociation. Finally, Au nanoparticles are found to show higher reactivity than Ag ones as long the oxidation of CO and the dissociation of NO_2. This unexpected behavior is due to the largest facility of the Au particle to deform in the presence of adsorbates which results in additional low coordinated sites.

Acknowledgments This work was supported by the Spanish MICINN grant CTQ2012-30751 and, in part, by the Generalitat de Catalunya 2014SGR97 XRQTC project. F.I acknowledges additional funding through the 2009 ICREA Academia award.

References

1. Haruta M (1997) Size- and support- dependency in the catalysis of gold. Cat Today 36:153–166
2. Valden M, Lai X, Goodman DW (1998) Onset of catalytic activity of gold clusters on Titania with the appearance of nonmetallic properties. Science 281:1647–1650
3. Wallace WT, Whetten RL (2002) Coadsorption of CO and O_2on selected gold clusters: evidence for efficient room-temperature CO_2 generation. J Am Chem Soc 124:7499–7505
4. Sanchez A, Abbet S, Heiz U, Schneider W-D, Hakkinen H, Barnett RN, Landman U (1999) When gold is not noble: nanoscale gold catalysts. J Phys Chem A 103:9573–9578
5. Iizuka Y, Tode T, Takao T, Yatsu K, Takeuchi T, Tsubota S, Haruta M (1999) A kinetic and adsorption study of CO oxidation over unsupported fine gold powder. J Catal 187:50–58

6. Herzing AA, Kiely CJ, Carley AF, Landon P, Hutchings GJ (2008) Nanoclusters on iron oxide supports for CO oxidation. Science 321: 1331–1335
7. Rodriguez JA, Illas F (2012) Activation of noble metals on metal-carbide surfaces: novel catalysts for CO oxidation, desulfurization and hydrogenation reactions. PhysChemChemPhys 14:427–438
8. Rodriguez JA, Evans J, Feria L, Vidal AB, Liu P, Nakamura K, Illas F (2013) CO_2 hydrogenation on Au/TiC, Cu/TiC and Ni/TiC catalysts: production of CO, methanol and methane. J Catal 307:162–169
9. Valden M, Pak S, Lai X, Goodman DW (1998) Structure sensitivity of CO oxidation over model Au/TiO2 catalysts. Cat Lett 56:7–10
10. Hvolbæk B, Janssens TVW, Clausen BS, Falsig H, Christensen CH, Nørskov JK (2007) Catalytic activity of Au nanoparticles. NanoToday 2(4):14–18
11. Roldán A, González S, Ricart JM, Illas F (2009) Critical Size for O_2 dissociation by Au nanoparticles. ChemPhysChem 10:348–351
12. Roldán A, Ricart JM, Illas F (2009) Influence of the exchange-correlation potential on the description of the molecular mechanism of oxygen dissociation by Au nanoparticles. Theor Chem Acc 123:119
13. Turner M, Golovko VB, Vaughan OPH, Abdulkin P, Berenguer-Murcia A, Tikhov MS, Johnson BFG, Lambert RM (2008) Selective oxidation with dioxygen by gold nanoparticle catalysts derived from 55-atom clusters. Nature 454:981–983
14. Gajdoš M, Hafner J, Eichler A (2006) *Ab initio* density-functional study of NO on close-packed transition and noble metal surfaces: I. Molecular adsorption. J Phys Condens Matter 18:13–40
15. Gajdoš M, Hafner J, Eichler A (2006) *Ab initio* density-functional study of NO adsorption on close-packed transition and noble metal surfaces: II. Dissociative adsorption. J Phys Condens Matter 18:41–54
16. Torres D, González S, Neyman KM, Illas F (2006) Adsorption and oxidation of NO on Au(111) surface: density functional studies. Chem Phys Lett 422:412–416
17. Lemire C, Meyer R, Shaikhutdinov S, Freund H-J (2004) Do quantum size effects control CO adsorption on gold nanoparticles? Angew Chem Int Ed 43:118–121
18. Ovesson S, Lundqvist BI, Schneider WF, Bogicevic A (2005) NO oxidation properties of Pt(111) revealed by *ab initio* kinetic simulations. Phys Rev B 71:115406 (1–5)
19. Gates BC (1995) Supported metal-clusters - synthesis, structure, and catalysis. Chem Rev 95:511–522
20. Ertl G (2008) Handbook of heterogeneous catalysis. Wiley-VCH, Weinheim
21. Anderson JA, Fernández-García M (2011) Supported metals in catalysis, 2nd edn. Catalytic science series: Vol 11, Imperial College Press, London
22. Viñes F, Gomes JRB, Illas F (2014) Understanding the reactivity of metallic nanoparticles: beyond the extended surface model for catalysis. Chem Soc Rev. doi:10.1039/c3cs60421g
23. Brønsted N (1928) Acid and basic catalysis. Chem Rev 5:231–338
24. Evans MG, Polanyi NP (1938) Inertia and driving force of chemical reactions. Trans Faraday Soc 34:11–24
25. Boudart M (1997) In:Ertl G, Knözinger H, Weitkamp J (eds.) Handbook of heterogeneous catalysis. Wiley-VCH, Weinheim, p 1
26. Logadottir A, Rod TH, Nørskov JK, Hammer B, Dahl S, Jacobsen CJH (2001) The brønsted–evans–polanyi relation and the volcano plot for ammonia synthesis over transition metal catalysts. J Catal 197:229–231
27. Viñes F, Vojvodic A, Abild-Pedersen F, Illas F (2013) Brønsted-evans-polanyi relationship for transition metal carbide and transition metal oxide surfaces. J Phys Chem C 117:41681
28. Grabow LC, Studt F, Abild-Pedersen F, Petzold V, Kleis J, Bligaard T, Norskov JK (2011) Angew Chem Int Ed 50:4601
29. Fajin JLC, Cordeiro MNDS, Illas F, Gomes JRB (2010) Descriptors controlling the catalytic activity of metallic surfaces towards water splitting. J Catal 276:92
30. Fajín JCL, Cordeiro MNDS, Illas F, Gomes JRB (2014) Generalized brønsted-evans-polanyi relationships and descriptors for O-H Bond cleavage of organic molecules on transition metal surfaces. J Catal 313:24
31. Kresse G, Hafner J (1993) Ab initio molecular-dynamics for liquid-metals. Phys Rev B47:558
32. Kresse G, Hafner J (1993) Ab initio molecular-dynamics for open-shell transition-metals. Phys Rev B 48:13115
33. Kresse G, Hafner J (1994) Ab initio molecular-dynamics simulation of the liquid-metal amorphous-semiconductor transition in germanium. Phys Rev B 49:14251
34. Kresse G, Furthmüller J (1996) Efficient iterative schemes for ab initio total-energy calculations using a plane-wave basis set. Phys Rev B 54:11169
35. Kresse G, Furthmüller J (1999) Efficiency of ab-initio total energy calculations for metals and semiconductors using a plane-wave basis set. Comp Mat Sci 6:15
36. Blöchl PE (1994) Projector augmented-wave method. Phys Rev B50: 17953
37. Perdew JP, Chevary JA, Vosko SH, Jackson KA, Pederson MR, Singh DJ, Fiolhais C (1992) Atoms, molecules, solids, and surfaces - applications of the generalized gradient approximation for exchange and correlation. Phys Rev B 46:6671–6687
38. Perdew JP, Chevary JA, Vosko SH, Jackson KA, Pederson MR, Singh DJ, Fiolhais C (1993) Atoms, molecules, solids, and surfaces: applications of the generalized gradient approximation for exchange and correlation (46:6671, 1992) Phys Rev B 48: 4978
39. Perdew JP, Burke K, Ernzerhof M (1996) Generalized gradient approximation made simple. Phys Rev Lett 77:3865–3868
40. Janthon P, Kozlov SM, Viñes F, Limtrakul J, Illas F (2013) Establishing the accuracy of broadly used density functionals in describing bulk properties of transition metals. J Chem Theory Comput 9:1631–1640
41. Zhao Y, Truhlar DG (2006) A new local density functional for main-group thermochemistry, transition metal bonding, thermochemical kinetics, and noncovalent interactions. J Chem Phys 125:194101
42. Ashcroft NW, Mermin ND (1976) Solid state physics. Saunders College Publishing, Orlando, p 335
43. Janthon P, Luo SA, Kozlov SM, Viñes F, Limtrakul J, Truhlar DG, Illas F (2013) Bulk properties of transition metals: a challenge for the design of universal density functionals. J Chem Theory Comput. doi: 10.1021/ct500532v
44. Grimme S (2006) Semiempirical GGA-type density functional constructed with a long-range dispersion correction. J Comp Chem 27: 1787–1799
45. Roldán A, Viñes F, Illas F, Ricart JM, Neyman KM (2008) Density functional studies of coinage metal nanoparticles: Scalability of their properties to bulk. Theor Chem Acc 120: 565
46. Monkhorst HJ, Pack JD (1976) Special points for brillouin-zone integrations. Phys Rev B 13:5188
47. Fajin JLC, Illas F, Gomes JRG (2009) Effect of the exchange-correlation potential and of surface relaxation on the description of the H_2O dissociation on Cu(111). J Chem Phys 130: 224702
48. Hollins P, Pritchard J (1979) Interactions of CO molecules adsorbed on Cu (111). Surf Sci 89:486–495
49. Vollmer S, Witte G, Wöll C (2001) Determination of site specific adsorption energies of CO on copper. Cat Lett 77: 97–101
50. Mc Elhiney G, Papp H, Pritchard J (1976) The adsorption of Xe and CO on Ag(111). Surf Sci 54:617–634
51. Elliot GS, Miller DR (1984) Proc 14th Int Symp on rare field gas dynamics. University of Tokyo Press, Tokyo, pp 349–358

52. Beret EC, Ghiringhelli LM, Scheffler M (2011) Free gold clusters: beyond the static, monostructure description. Faraday Discuss 152: 153–167
53. Beret EC, van Wijk MM, Ghiringhelli LM (2014) Reaction cycles and poisoning in catalysis by gold clusters: a thermodynamics approach. Int J Quantum Chem 114:57–65
54. Habas M-P, Mele F, Sodupe M, Illas F (1999) Density functional cluster model study of bonding and coordination modes of CO_2 on Pd(111). Surf Sci 431:208–219
55. Rodriguez AH, Branda MM, Castellani NJ (2006) DFT studies of the adsorption and interaction of two methanol molecules on a MgO edge. THEOCHEM 769:249–254